Draft version March 7, 2016
Preprint typeset using LaTeX style emulateapj v. 5/2/11

PHOTOMETRIC SUPERNOVA CLASSIFICATION WITH MACHINE LEARNING

Michelle Lochner[1], Jason D. McEwen[2], Hiranya V. Peiris[1], Ofer Lahav[1], Max K. Winter[1]
[1]Department of Physics and Astronomy, University College London, Gower Street, London WC1E 6BT, UK and
[2]Mullard Space Science Laboratory, University College London, Surrey RH5 6NT, UK

Draft version March 7, 2016

ABSTRACT

Automated photometric supernova classification has become an active area of research in recent years in light of current and upcoming imaging surveys such as the Dark Energy Survey (DES) and the Large Synoptic Survey Telescope (LSST), given that spectroscopic confirmation of type for all supernovae discovered with these surveys will be impossible. Here, we develop a multi-faceted classification pipeline, combining existing and new approaches. Our pipeline consists of two stages: extracting descriptive features from the light curves and classification using a machine learning algorithm. Our feature extraction methods vary from model-dependent techniques, namely SALT2 fits, to more independent techniques fitting parametric models to curves, to a completely model-independent wavelet approach. We cover a range of representative machine learning algorithms, including naive Bayes, k-nearest neighbors, support vector machines, artificial neural networks and boosted decision trees. We test the pipeline on simulated multi-band DES light curves from the Supernova Photometric Classification Challenge. Using the commonly-used area under the Receiver Operating Characteristic curve (AUC) as a metric, we find that the SALT2 fits and the wavelet approach, with the boosted decision trees algorithm, each achieves an AUC of 0.98, where 1 represents perfect classification. We find that a representative training set is essential for good classification, whatever the feature set or algorithm, suggesting that spectroscopic follow-up is best focused on fewer objects at a broad range of redshifts than on many bright objects. Importantly, we find that by using either one of the two best feature extraction methods (SALT2 model fits and wavelet decomposition) and a boosted decision tree algorithm, accurate classification is possible purely from light curve data, without the need for any redshift information.

Subject headings: methods:data analysis — cosmology:observations — supernovae:general

1. INTRODUCTION

Astronomy is entering an era of deep, wide-field surveys and massive datasets, which requires the adoption of new, automated techniques for data reduction and analysis. In the past, supernova datasets were small enough to allow spectroscopic follow-up for the majority of objects, confirming the type of each. Only type Ia's are currently used for cosmology, and the type is of course required for astrophysical modeling and studies. With the onset of surveys such as the Dark Energy Survey (DES) (Dark Energy Survey Collaboration 2005; Dark Energy Survey Collaboration et al. 2016) and the upcoming Large Synoptic Survey Telescope (LSST) (LSST Science Collaboration 2009), only a small fraction of the dataset can be spectroscopically followed up. The current commonly used dataset, the Joint Light curve Analysis (JLA) (Betoule et al. 2014), contains only 740 supernovae, while DES is expected to detect thousands (Bernstein et al. 2012) and LSST hundreds of thousands (LSST Science Collaboration 2009) of supernovae. Thus alternative approaches to supernova science must be developed to leverage these largely photometric datasets.

Supernova cosmology is possible without strictly knowing the supernova type using, for example, Bayesian methods (M. Kunz, B. Bassett and R. Hlozek 2007; R. Hlozek et al. 2012; J. Newling et al. 2012; Knights et al. 2013; Rubin et al. 2015). However, these techniques benefit from having a reasonable probability for the type of each object in the dataset, so some form of probabilistic classification is useful. Additionally, studies of core-collapse supernovae and other transients rely on good photometric classification. Further, the observing strategy for LSST has not yet been finalized and the effect of observing strategy on supernova classification has not yet been established. Here we outline a multi-faceted pipeline for photometric supernova classification. In future work, we will apply it to LSST simulations to understand the effect of observing strategy on classification.

Current photometric supernova classification techniques focus on empirically-based template fitting (Sako et al. 2008; Sako et al. 2014). However, in the past few years there have been several innovative techniques proposed to address this problem (see Kessler et al. (2010b) and references therein).

Here, we apply machine learning to this problem, as a well-established method of automated classification used in many disciplines. As astronomical datasets become larger and more difficult to process, machine learning has become increasingly popular (Ball & Brunner 2010; Bloom & Richards 2012). Machine learning techniques have been proposed as a solution to an earlier step in the supernova pipeline, that of classifying transients from images (du Buisson et al. 2015; Wright et al. 2015). Machine learning is also already being employed at some level for photometric supernova classification in the Sloan Digital Sky Survey (SDSS) (Frieman et al. 2008; Sako et al. 2008), using the parameters from template-fitting as features (Sako et al. 2014).

Contact email: dr.michelle.lochner@gmail.com

We investigate the effect of including host galaxy photometric redshift information in automated classification. Reliable redshifts are important for current classification techniques in order to reliably fit the templates. However, for future surveys such as LSST, well-constrained, unbiased redshifts may be difficult to obtain and could negatively affect classification. A classification technique which is independent of redshift information could therefore be invaluable.

Additionally, we investigate the effect of providing the machine learning algorithms with a non-representative training set. In general, one would expect the spectroscopically confirmed training set to be biased in terms of brightness (and hence redshift) because it is far easier to obtain spectra for brighter objects. However, any classification technique is likely to underperform with a biased training set. In our analysis, we explore both representative and non-representative training sets.

In this paper, we investigate four different methods of extracting useful features from light curves, as well as five representative machine learning algorithms. In Sec. 2 we summarize the simulated dataset used. Sec. 3 explains our feature extraction methods, varying from highly model dependent approaches to a completely model independent method. Section 4 introduces the machine learning algorithms used in this work. We present our results in Sec. 6 and conclude in Sec. 7.

2. SUPERNOVA SIMULATIONS

To test and compare methods, we use existing supernova simulations from the Supernova Photometric Classification Challenge (SPCC) (Kessler et al. 2010a,b), which are simulated DES light curves built from an existing library of non-Ia templates and using both SALT2 (Guy et al. 2007) and MLCS2k2 (Jha et al. 2007) type Ia models. Simulated photometric host galaxy redshifts are available for each object and we investigate the effect of withholding this information from the machine learning algorithms, in order to see if redshift is an essential ingredient for classification. We have not tested whether or not the results would improve if spectroscopic redshifts were available, since for DES and LSST this is an unlikely scenario.

In the original challenge, a training set of 1103 spectroscopically-confirmed objects was provided while a test set of 20216 objects was retained to compare the techniques under study. It is important to note that this training set is non-representative in brightness and hence also in redshift. This was done to emulate the way spectroscopic follow-up is currently performed, which prioritizes bright objects. We return to this point in Sec. 6. Figure 1 shows an example type Ia light curve from the challenge data.

3. EXTRACTING USEFUL LIGHT CURVE FEATURES

Feature extraction is a crucial step in the machine learning process. Raw data almost inevitably requires dimensionality reduction or some form of summarizing of key features in the data, and very few data sets can be successfully classified in a raw format. Good feature extraction techniques will produce a feature set of much lower dimensionality than the original data with features that adequately describe the original data and are well-separated between classes. Examples of commonly used features include principal component analysis (PCA) (Pearson 1901; Hotelling 1933) coefficients or derived quantities such as amplitude, period, phase etc. For a general overview of feature extraction see Li et al. (2016).

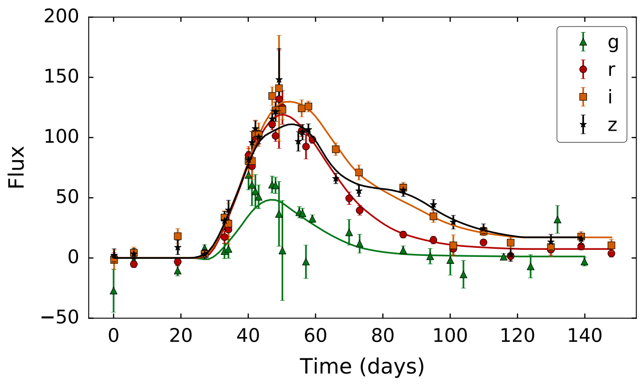

Fig. 1.— An example simulated DES type Ia supernova light curve (object ID 009571), at redshift 0.42, from the Supernova Photometric Classification Challenge (Kessler et al. 2010a,b). The photometric light curve is measured in the four DES *griz* filter bands, showing the rise in brightness after the explosion of the star and subsequent decay. The points and error bars are the data points, while the curves are from the best fitting SALT2 model (see Sec. 3).

We test a variety of feature sets and evaluate their performance based on the effectiveness of subsequent classification for a variety of machine learning algorithms. Alternative feature selection approaches agnostic of machine learning algorithms could be considered, although as these approaches evaluate the feature sets in isolation, they could lead to biases after a machine learning algorithm is applied. A detailed investigation of alternative approaches to choosing and evaluating features is beyond the scope of this article.

We explore three different, broad approaches to feature extraction, ranging from a highly model-dependent method based on supernova templates to a completely model-independent wavelet based approach, with a parametric approach somewhere in between. These bracket a wide range of approaches one could consider using to extract features from light curves. We run a pipeline whereby we extract the four feature sets from the same data, and then run five different machine learning algorithms (described in Sec. 4) on each feature set to compare performance.

Before discussing the feature extraction methods we have studied, we introduce a useful visualization technique for understanding feature sets.

3.1. *Visualizing feature sets with t-distributed stochastic neighbor embedding*

Although feature extraction generally reduces dimensionality from raw data, the number of features often remains large, making it difficult to determine whether or not they have good separability. t-Distributed stochastic neighbor embedding (t-SNE) (Van der Maaten & Hinton 2008) is a sophisticated technique designed to produce a low-dimensional representation of a high-dimensional space, whilst clustering similar features together. t-SNE works by first computing, for each pair of points, the probability that the two points are similar based on their Euclidean distance. The aim then is to find the cor-

TABLE 1
Priors on the SALT2 model parameters.

Parameter name	Prior
z	$\mathcal{U}(0.01, 1.5)$
t_0	$\mathcal{U}(-100, 100)$
x_0	$\mathcal{U}(-10^{-3}, 10^{-3})$
x_1	$\mathcal{U}(-3, 3)$
c	$\mathcal{U}(-0.5, 0.5)$

responding low-dimensional values for these points that preserves the same probability. Stochastic neighbor embedding (SNE) determines these values by minimizing the sum of Kullback-Leibler divergences (a simple measure of divergence between probability distributions) over all data points, using a gradient descent algorithm. t-SNE differs from SNE in the choice of exact probability distribution defining the similarity between points (using a Student-t distribution instead of a Gaussian) and in the exact choice of cost function to minimize (see Van der Maaten & Hinton (2008) for details). If the embedded features are well-separated on the t-SNE plot, one can generally expect accurate classification. However, the converse is not strictly true and poorly-separated features may still be well-classified with a sophisticated machine learning algorithm. Each of the feature extraction methods discussed below has an accompanying t-SNE plot for visualization purposes (Fig. 3.2).

3.2. *Template fitting approach to classification*

Historically, classification of photometric supernovae (generally used to identify candidates for spectroscopic follow-up) has focused on the use of supernova templates constructed from existing data sets of supernovae (Sako et al. 2008). Light curve features such as stretch and color parameters have been used to classify photometric supernovae from SDSS (Sako et al. 2011). We choose the SALT2 (Spectral Adaptive Light curve Template 2) model (Guy et al. 2007) of type Ia supernovae as it is the most commonly used.

In the SALT2 model, the flux in a given band of a type Ia light curve is given by

$$\begin{aligned} F(t,\lambda) = x_0 \times [M_0(t,\lambda) + x_1 M_1(t,\lambda) + ...] \\ \times \exp[c\mathrm{CL}(\lambda)], \end{aligned} \tag{1}$$

where t is the phase (time since maximum brightness in the B-band), λ is the rest frame wavelength, $M_0(t,\lambda)$ is average spectral sequence (using past supernova data as described in Guy et al. 2007), and $M_k(t,\lambda)$ for $k > 0$ are higher order components to capture variability in the supernovae. In practice, only $M_0(t,\lambda)$ and $M_1(t,\lambda)$ are used. $CL(\lambda)$ is the average color correction law. For each object, the redshift z is also used as either a given or fitted parameter. Thus this method has 5 features: z, t_0 (the time of peak brightness in the B-band), x_0, x_1 and c. We use the implementation of SALT2 in `sncosmo`[1] (Barbary 2014) and obtain the best fitting parameters using `MultiNest`[2] (Feroz & Hobson 2008; Feroz et al. 2009, 2013) with the `pyMultiNest`[3] (Buchner, J. et al. 2014) software. Table 1 lists the priors used on all parameters.

[1] http://sncosmo.readthedocs.org/en/v1.2.x/
[2] https://ccpforge.cse.rl.ac.uk/gf/project/multinest/
[3] https://johannesbuchner.github.io/PyMultiNest/

Figures 2(a) and 2(b) show the t-SNE plots for the SALT2 features both without and with redshift information. The t-SNE plots show a lot of structure, partly due to the relative low-dimensionality of the feature space, which corresponds to a highly constrained 2D plot. The features are fairly well-separated, especially when redshift is included, but it is clear that it is difficult to distinguish between type Ia and Ibc supernovae.

3.3. *General parametric approach to classification*

The template-fitting approach relies on a significant amount of prior knowledge about supernovae. An alternative is to use a more general parametric description and use the fitted parameters as features in the machine learning pipeline. We use two different parametric models that have been proposed in the literature as good parameterizations of a supernova light curve and were both used in solutions to the SPCC. Model 1 is the parameterization used in Newling et al. (2011), while Model 2 is proposed in Karpenka et al. (2013).

We use these models because they are both proposed solutions to precisely the problem of supernova classification. While similar, the models have some differences, especially in the treatment of the tail of the light curves, the ability to describe double peaks and the small difference in number of parameters, which makes it interesting to compare them.

We also considered the linear piecewise model proposed in Sanders et al. (2015) but found that the relatively large number of parameters (11 per filter) made it less robust when fitting to data, and consequently classification with this feature set did not typically perform well.

3.3.1. *Model 1*

The model used in Newling et al. (2011) describes the flux of a supernova (in any band) by

$$F(t) = A\left(\frac{t-\phi}{\sigma}\right)^k \exp\left(-\frac{t-\phi}{\sigma}\right) k^{-k} e^k + \Psi(t), \tag{2}$$

where

$$\Psi(t) = \begin{cases} 0 & -\infty < t < \infty \\ \text{cubic spline} & \phi < t < \tau \\ \psi & \tau < t < \infty \end{cases}, \tag{3}$$

and $A + \psi$ is the peak flux, ϕ is the starting time of the explosion, k governs the relative rise and decay times of the light curve and σ is the width or 'stretch' of the light curve. The time of the peak flux, τ, is given by $\tau = k\sigma + \phi$. The function $\Psi(t)$ is a 'tail' function that ensures that the flux tends to a finite value as $t \to \infty$ and the cubic spline is determined to have zero derivative at $t = \phi$ and $t = \tau$.

Each filter band is fitted individually with these five parameters (A, ϕ, σ, k, ψ), giving a total of 20 features for each object (or 21 if redshift is included). The parameters are all fitted with `MultiNest`, as in Sec. 3.2, and the best fit is taken to be the maximum posterior value for each parameter. The priors on the parameters (which are the same for all four filter bands) are given in Table 2.

Figures 2(c) and 2(d) show the t-SNE plots for the Model 1 feature set both without and with redshift in-

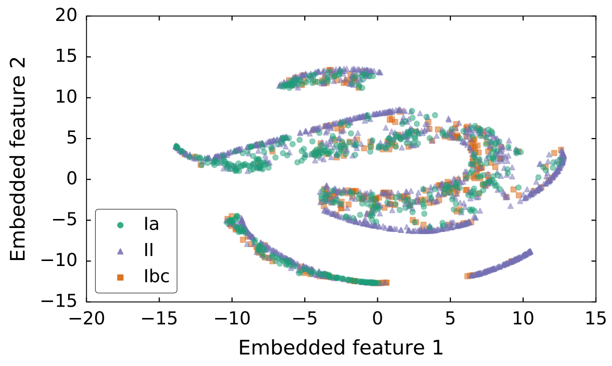

(a) SALT2 without redshift (5 features)

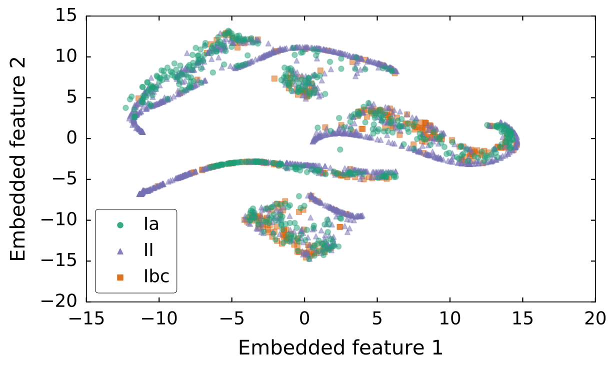

(b) SALT2 with redshift (5 features)

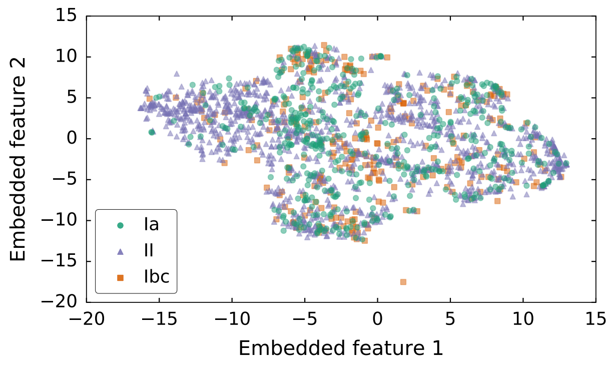

(c) Parametric Model 1 without redshift (20 features)

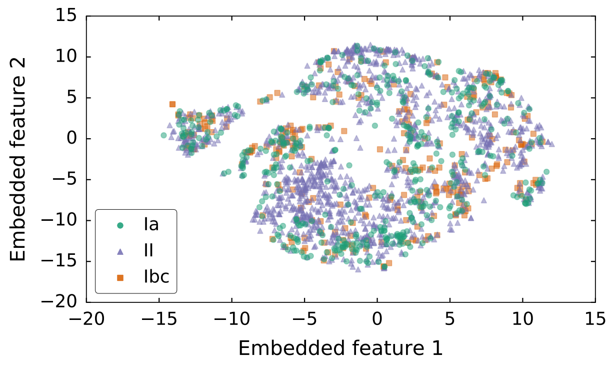

(d) Parametric Model 1 with redshift (21 features)

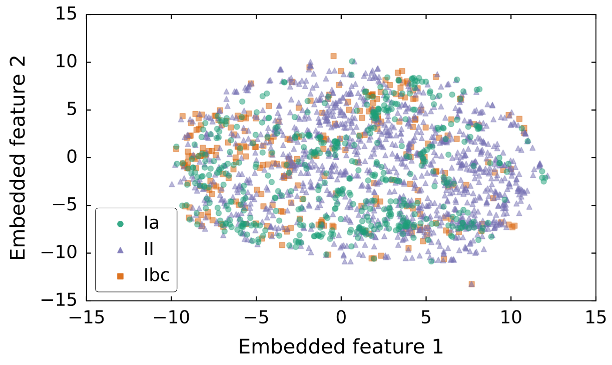

(e) Parametric Model 2 without redshift (24 features)

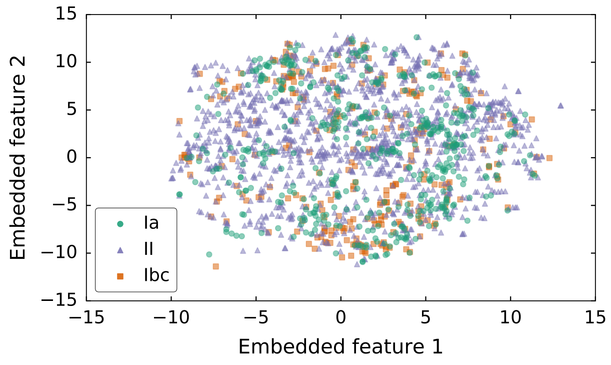

(f) Parametric Model 2 with redshift (25 features)

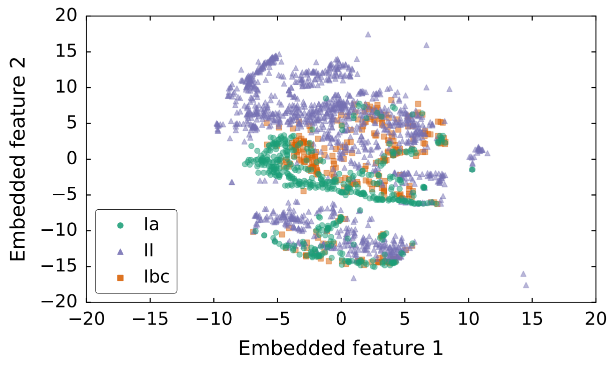

(g) Wavelets without redshift (20 features)

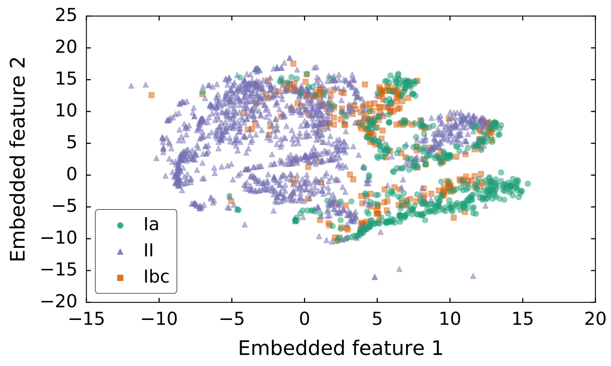

(h) Wavelets with redshift (21 features)

Fig. 2.— t-SNE (t-distributed stochastic neighbor embedding) visualizations for feature sets with and without redshift information. This is a two-dimensional visualization of the high-dimensional feature space. Each of the three classes of supernovae is represented by a different color; if the classes are well-separated in the embedding space, we would expect these features to provide good classification. Note that all units are arbitrary and the original dimensionality is indicated in brackets.

TABLE 2
Priors on the Model 1 parameters.

Parameter name	Prior
$\log(A)$	$\mathcal{U}(0, 10)$
ϕ	$\mathcal{U}(-60, 100)$
$\log(\sigma)$	$\mathcal{U}(-3, 4)$
$\log(k)$	$\mathcal{U}(-4, 4)$
$\log(\psi)$	$\mathcal{U}(-6, 10)$

formation respectively. In both cases, the features do not appear to be easily separable.

3.3.2. *Model 2*

The proposed parameterization from Karpenka et al. (2013) is similar to Model 1 but allows for the possibility of double peaks in light curves. The flux is given by

$$F(t) = A\left[1 + B(t - t_1)^2\right] \frac{\exp[-(t - t_0)/T_{\rm fall}]}{1 + \exp[-(t - t_0)/T_{\rm rise}]}, \quad (4)$$

where t is assumed to be the earliest measurement in the r-band light curve. We again fit all parameters using `MultiNest` and take the maximum posterior parameters. There are 6 parameters per filter band, thus forming a feature set of 24 features (or 25 including redshift) for each object. We use the same priors as in Karpenka et al. (2013), given in Table 3.

TABLE 3
Priors on the Model 2 parameters.

Parameter name	Prior
$\log(A)$	$\mathcal{U}(\log(10^{-5}), \log(1000))$
$\log(B)$	$\mathcal{U}(\log(10^{-5}), \log(100))$
t_0	$\mathcal{U}(0, 100)$
t_1	$\mathcal{U}(0, 100)$
$T_{\rm rise}$	$\mathcal{U}(0, 100)$
$T_{\rm fall}$	$\mathcal{U}(0, 100)$

The t-SNE plots for the Model 2 features can be seen in Fig. 2(e) and Fig. 2(f) without and with redshift respectively. As in Model 1, the features do not appear to be well-separated.

3.4. *Wavelet decomposition approach to classification*

While the model-dependent approaches to feature extraction considered so far are useful for incorporating prior information about SN light curves, they are sensitive to mis-specification of light curve models. It is quite possible important light curve characteristics cannot be captured efficiently by simple models, such as Models 1 and 2 described above. A model-independent, non-parametric approach to feature extraction is therefore required as a complementary approach that is not dependent on prior information.

A wavelet decomposition is a good choice for feature extraction since certain wavelet transforms can be constructed that are approximately invariant under translation and stretch. One could then expect the wavelet coefficients of the light curves of two similar supernovae measured at different times, or two similar objects at different redshifts, to themselves be similar. Recently, Varughese et al. (2015) have shown that a wavelet-based approach to photometric supernova classification can be highly effective. Here we consider a substantially different method in the actual wavelet decomposition of the light curves and subsequent classification, but also find wavelets to be an excellent feature extraction method.

The procedure we follow to extract features using wavelets is to first interpolate the light curves onto the same grid of points (using Gaussian processes), then to perform a redundant wavelet decomposition, and lastly to use PCA to reduce the dimensionality of the feature set.

3.4.1. *Interpolation using a Gaussian process regression*

In order to perform a wavelet decomposition, all light curves are interpolated onto the same uniform grid of points. We use Gaussian process regression since it has the advantage over (for example) spline interpolation in that it allows the straightforward inclusion of uncertainty information and produces a less biased estimate of interpolated values.

A Gaussian process is the generalization of a Gaussian distribution, forming a distribution for which each point of the input variable is associated with a normally-distributed random variable (MacKay 2003). A Gaussian process is fully specified by a mean function of the input variable (time, in the case of a light curve) and a covariance function, which specifies the covariance between values of the function at pairs of points in time. Gaussian process regression then proceeds by determining the mean function and hyperparameters of the covariance matrix. We use the package `GaPP`[4] used in Seikel et al. (2012) to perform the Gaussian process regression of each of the light curves.

3.4.2. *Wavelet decomposition*

Wavelet transforms are an invaluable tool in signal analysis due to the ability of wavelets to to localize signal content in scale and time simultaneously, whereas real space or Fourier representations provide signal localization, respectively, in time or frequency only (see Valens (1999) for a gentle introduction to wavelets). For the continuous wavelet transform (CWT), the set of wavelet atoms forming the transform dictionary are scale- and translation-invariant, i.e., a scaled or translated atom also belongs to the dictionary, hence the CWT achieves scale- and translation-invariance (Mallat 2009). However, the discrete wavelet transform (DWT), which permits fast transforms and exact synthesis from a finite, discrete set of wavelet coefficients, suffers from a lack of translation-invariance due to the critical sub-sampling performed. Approximate translation-invariance can be achieved by eliminating sub-sampling from the DWT, leading to the redundant à trous wavelet transform (Holschneider et al. 1989; Mallat 2009), which is also called the stationary wavelet transform.

We adopt the à trous wavelet transform, which also achieves dyadic scale-invariance, and use the symlet family of wavelets, which are a more symmetric version of the widely-used Daubechies family of wavelets (Daubechies 1988). We use the implementation provided in the `PyWavelets`[5] software package. Our results were found

[4] http://www.acgc.uct.ac.za/~seikel/GAPP/main.html
[5] http://www.pybytes.com/pywavelets/contents.html

not to be highly dependent on the family of wavelet chosen. Alternative wavelet constructions that achieve better translation- and scale-invariance could be considered (e.g. Kingsbury 2001; Lo et al. 2009; Xiong et al. 2000) but a detailed optimization of the wavelet transform used was not performed, highlighting the robustness of our approach.

For this work, we used 100 points on the Gaussian process curve and a two-level wavelet transform, returning 400 (highly redundant) coefficients per filter, or 1600 coefficients per object.

3.4.3. *Dimensionality reduction with PCA*

The output of the wavelet decomposition is highly redundant (which preserves translation invariance) and thus extremely high-dimensional. The final step in the process is to run a PCA to reduce dimensionality. PCA is a linear transform that transforms a set of correlated variables into linearly uncorrelated variables using singular value decomposition of the matrix of variables. From this, a set of eigenvectors (components) and eigenvalues are obtained. The components with large eigenvalues describe the majority of the variability of the dataset and dimensionality reduction is achieved by discarding components with negligible eigenvalues. After PCA, we reduce the dimensionality of the feature set from 1600 to 20 dimensions whilst retaining 98% of the information in the dataset (as measured by determining the fraction of the sum of eigenvalues of components retained to that of all components).

We show the t-SNE plots for the wavelet features without and with redshift in Fig. 2(g) and Fig. 2(h). Here, the features seem encouragingly well-separated between classes, even between type Ia and Ibc in some parts of feature space. We would thus expect the wavelet features to perform well in classification.

4. MACHINE LEARNING FOR CLASSIFICATION

Machine learning is a powerful tool for modern astronomy (Bloom & Richards 2012; Ball & Brunner 2010), becoming increasingly popular in the era of massive data sets. It allows the automation of tasks previously performed by humans and also, as in this case, allows the classification of objects that are seemingly inseparable to the human eye. Supervised machine learning algorithms learn a mapping function from training data to allow them to classify new test objects. A large variety of machine learning algorithms exist, and it is beyond the scope of this paper to consider each one. Instead, we consider five popular machine learning algorithms that are fairly representative of the main approaches used. All these algorithms and several others are comprehensively compared in Caruana & Niculescu-Mizil (2006), who find (as we do) that boosted decision trees and random forests often outperform other classifiers for many problems. For all algorithms, we use the Python package `scikit-learn`[6] (Pedregosa et al. 2011). The selected algorithms used are able to compute not just the classification of a particular object, but also a classification probability, which allows one to construct a final dataset of the desired purity by changing the threshold probability for belonging to the class of interest.

[6] `http://scikit-learn.org/`

4.1. *Description of machine learning algorithms*

The algorithms used in this work are: naive Bayes (a basic probabilistic classifier), k-nearest neighbors (a classifier based on clustering of features), a multilayer perceptron (the simplest form of artificial neural network), a support vector machine (which works by finding a separating hyperplane between classes) and boosted decision trees (an ensemble method that combines a multitude of decision trees, a weaker classifier). What follows is a brief overview of the five algorithms considered, in each case referring the reader to references for more details.

4.1.1. *Naive Bayes (NB)*

Given a set of features for an object, $x_1, x_2, ...x_n$, the Naive Bayes (NB) algorithm (Zhang 2004) states that the probability of that object belonging to class y is

$$P(y|x_1, ..., x_n) \propto P(y) \prod_i P(x_i|y), \quad (5)$$

assuming independence between features. $P(y)$ can be estimated by determining the frequency of y in the training set. In the implementation of NB that we use, the likelihood, $P(x_i|y)$, is assumed to be Gaussian, the parameters of which are determined from the training data by maximizing the likelihood. The predicted class is simply determined to be the class that maximizes Eq. (5).

The advantage of NB is that it is fast and scales very well to high dimensions. The disadvantage is that it assumes independence between features and that the features are Gaussian-distributed. One or both of these assumptions is frequently broken.

4.1.2. K-*Nearest neighbors (KNN)*

K-Nearest neighbors (KNN) (Altman 1992) is a simple algorithm which classifies an object by performing a majority vote of the classes of the k nearest neighbors. We use a Euclidean distance measure to determine the nearest neighbors, applying a weight to each neighbor inversely proportional to the distance.

The probability of an object belonging to class y is found by summing the weights of all neighbors also belonging to class y and dividing by the sum of the weights of all neighbors. The advantage of KNN is its relative simplicity and its use as a clustering, unsupervised learning algorithm. The disadvantages are that it is computationally intensive for large datasets, given that all pairwise distances have to be calculated; further, the results are highly dependent on the exact training set used, making the results fairly inconsistent especially for small training sets.

4.1.3. *Artificial neural networks (ANN)*

Artificial neural networks (ANN) (Jeffrey & Rosner 1986) are a family of machine learning algorithms inspired by biological systems of interconnected neurons. The aim of an ANN is to learn a non-linear function to map input features to output classes. For this work we use the commonly-used multi-layer perceptron (MLP) implemented in `scikit-learn`.

Each neuron transforms the inputs of the previous layer by constructing a weighted sum of the features, followed by some non-linear activation function, in this case a hyperbolic tan function. While in theory different topologies could be used, the MLP is constructed as a series of layers of neurons. In each layer, each neuron is connected to all the neurons of the previous layer, but not any others.

The standard topology is: $n \rightarrow h_1 \rightarrow h_2 \ldots h_m \rightarrow c$, where n is the number of input features, h_i is the number of neurons in layer i and c is the final class. For this problem, we find it does not improve performance to add more than one hidden layer. The `scikit-learn` implementation of a MLP uses backpropagation (Werbos 1974) to determine the weights.

The probability of an object belonging to a particular class is easily estimated from a MLP by normalizing the final activation function values so that they sum to one, thus treating them as probabilities. Neural networks have the advantage of being capable of learning highly non-linear mappings, often allowing highly accurate classifications. One disadvantage of neural networks is their sensitivity to tuning of hyperparameters such as number of hidden layers and the number of nodes in each layer.

4.1.4. *Support vector machines (SVM)*

Support vector machines (SVM) (Cortes & Vapnik 1995) are a type of classifier that works by finding the hyperplane in feature space that best separates classes (Ball & Brunner 2010). This hyperplane is defined by the vectors to the data points nearest the hyperplane, called the support vectors. Linear SVMs can be extended to the non-linear case by using the kernel trick (Aızerman 1964) to transform the features to a high-dimensional space so that non-linear relationships become linear. For this work, we use a radial basis function as a kernel, which is a Gaussian function of the Euclidean distance between features of different objects.

Probabilities from an SVM can be obtained using Platt scaling (Platt et al. 1999), which performs a logistic regression of the SVM's decision function scores. Platt scaling is computationally intensive, requiring an extra cross-validation step to determine the parameters of the transformation function. SVMs perform extremely well in general, even in high dimensions, and are highly versatile as different kernel functions can be considered to improve feature separation in any particular problem. The disadvantage of SVMs lies largely in their computational complexity when computing probabilities (if required).

4.1.5. *Boosted decision trees (BDT)*

Random forests (Breiman 2001) and boosted decision trees (Friedman 2002) are ensemble methods built up of a multitude of decision trees (Morgan & Sonquist 1963; Breiman et al. 1984).

Decision trees construct a model to map input features to output classes using a series of decision rules (Ball & Brunner 2010). In our case, the decisions are based on whether or not a given feature is in a particular range. The tree is trained by recursively selecting which feature and boundary gives the highest information gain in terms of classification. The problem with decision trees is that the trees created are often complex and do not generalize well beyond the training set, leading to over-fitting. They are also sensitive to small changes in the data, leading to large variance in predicted classes.

These problems can be overcome by combining decision trees in an ensemble method. Ensemble learning creates a multitude of decision trees on different subsets of data and averages the resulting classifications. There are two main approaches of combining classifiers: boosting and bagging. Random forests are created by bagging, which selects subsets of data with replacement (randomly in the case of random forests) on which to perform the classification. Boosting repeatedly fits the same dataset but with each iteration, it increases the weights of incorrectly classified objects, meaning subsequent classifiers focus on difficult cases. We found boosted decision trees (using the AdaBoost algorithm (Freund & Schapire 1997)) gave the same performance as bagging and were marginally faster in this case.

Probabilities are straightforward to estimate from decision trees: the probability of belonging to a given class is simply proportional to the fraction of trained objects in that class on the corresponding leaf of the tree. With an ensemble method, the probabilities from each of the decision trees in the ensemble is averaged to produce a final probability. Boosted decision trees are in general excellent classifiers (Dietterich 2000). Averaging over a large number of classifications makes them robust and unbiased estimators. The disadvantage is that they can be computationally intensive, although their computation time is still comparable to SVMs and ANNs.

4.2. *Interpreting machine learning results*

There are a variety of metrics for measuring the performance of a machine learning algorithm. Every machine learning algorithm we consider returns a probability for each classification. It is common to produce a set of predicted classifications by simply selecting, for each object, the class associated with the highest probability. However, this is not the full picture, as one can always obtain a more pure (but less complete) sample by varying the threshold probability at which an object is considered to be of a given class. Many metrics common in machine learning literature (such as purity or completeness) will depend on this subjective threshold and can be optimized for a specific class or goal (for example, obtaining a pure sample of type Ia supernovae for cosmology). Here we use a more general metric, receiver operating characteristic (ROC) curves, to directly compare algorithms.

4.3. *Receiver operating characteristic (ROC) curves*

A confusion matrix is useful for understanding most commonly used machine learning metrics. For a binary classification of two classes, positive and negative, the confusion matrix is shown in Table 4. An ideal classifier would produce only true positives without any contamination from false positives or losses from false negatives. In reality, any classification problem has a trade-off between purity and completeness.

An excellent method of comparing machine learning algorithms and visualizing this trade-off is to use ROC curves (Green & Swets 1966; Hanley & McNeil 1982; Spackman 1989) (see Fawcett (2004) for an introductory tutorial). These allow one to get an overview of the algorithms without having to select an arbitrary probability threshold at which to consider an object as belonging to a particular class. ROC curves can only compare one

TABLE 4
Confusion matrix for a classification problem with two classes: positive (P) and negative (N).

		True class	
		P	N
Predicted class	P	True positive (TP)	False positive (FP)
	N	False negative (FN)	True negative (TN)

class (assumed to be the desired class) against all others, but can easily be constructed for each class in turn. In this paper, all ROC curves are plotted assuming the binary classification of type Ia vs. non-Ia.

ROC curves are constructed by comparing the true positive rate against the false positive rate, as the probability threshold is varied. The true positive rate (TPR), also called recall, sensitivity or completeness, is the ratio between the number of correctly classified positive objects and the total number of positive objects in the data set,

$$\mathrm{TPR} = \frac{\mathrm{TP}}{\mathrm{TP} + \mathrm{FN}}. \tag{6}$$

The false positive rate (FPR), also referred to as the false alarm rate or 1− specificity, is the ratio between the number of objects incorrectly classified as positive and the total number of negative objects in the data set,

$$\mathrm{FPR} = \frac{\mathrm{FP}}{\mathrm{FP} + \mathrm{TN}}. \tag{7}$$

It is straightforward to see that a good classification algorithm will maximize the true positive rate (thus resulting in a more complete data set) while simultaneously minimizing the false positive rate (thus reducing contamination). The area-under-the-curve (AUC) of a ROC curve provides a straightforward way to directly compare classifiers. An AUC of 1 represents perfect classification, visually represented by a curve which reaches the top left corner. By contrast, a diagonal line would correspond to an AUC of 0.5, meaning the classifier does no better than random. In the machine learning literature, an AUC higher than 0.9 typically indicates an excellent classifier.

In Sec. 6 we use ROC curves to examine the differences between machine learning algorithms and our three different approaches to feature extraction.

4.4. *Purity and completeness*

Commonly-used metrics for classification include purity and completeness. These are only defined for classified objects, meaning some choice of probability threshold must be made. Usually, an object's class is selected as that with the highest probability. A more pure subset can be obtained by applying a high threshold probability. For any subset chosen, it is useful to determine the purity and completeness to evaluate it.

We can use the confusion matrix in Table 4 to define purity (also known as precision) as

$$\mathrm{purity} = \frac{\mathrm{TP}}{\mathrm{TP} + \mathrm{FP}} \tag{8}$$

and the completeness, which is equivalent to the TPR, as

$$\mathrm{completeness} = \frac{\mathrm{TP}}{\mathrm{TP} + \mathrm{FN}}. \tag{9}$$

4.5. *Algorithm parameter choices*

In supervised learning, the data are split into a training set, where each object has a known class label, and a test set, with unknown objects on which the classifier is run. Choice of training set is crucial, as a training set which is not representative of the entire dataset can dramatically decrease a classifier's performance (see Sec. 6). Additionally, almost all machine learning algorithms have hyperparameters that need to be optimized. In this work, we use five-fold cross-validation (Kohavi et al. 1995) to determine the values of the hyperparameters (see Table 5 for some example parameter values).

Cross-validation involves repeatedly dividing the dataset into randomly chosen training and *validation* sets. Over a grid of hyperparameter values, cross-validation uses each validation set to evaluate the performance of the classifier, finding the hyperparameters that maximize the AUC.

5. PHOTOMETRIC SUPERNOVA CLASSIFICATION PIPELINE

For each of the four feature sets (Sec. 3) and five machine learning algorithms (Sec. 4) considered, we perform the following procedure.

We split the data into a training and a test set, considering both a representative and a non-representative training set separately. The non-representative training set is the same as the one used in the SPCC. For a representative training set, we randomly select a set of objects the same size as the one in the challenge (1103 objects). We were able to repeat the representative case by randomly drawing several new training sets and running the full pipeline to see by how much results vary. We did not attempt to create a new non-representative training set with the same properties as the original.

In the SPCC, photometric host galaxy redshift information was provided, so we also investigate the importance of redshift information by running the full pipeline with all four feature extraction methods both with and without redshift. This is important because accurate photometric redshifts are difficult to obtain and the sensitivity of current and proposed classification techniques to the presence of redshift information has not yet been established. In the case of parametric models 1 and 2 and the wavelet decomposition, the redshift is simply added as an additional feature. For the SALT2 case, we fix the redshift in the model to the photometric redshift instead of allowing it to vary, thus better constraining the other parameters for type Ia's.

Before running any machine learning algorithm, we rescale the features with a standard scaling. We scale the features by removing the mean (centering on zero) and scaling to unit variance (dividing by the standard deviation). After rescaling, we run each of the machine learning algorithms outlined in Sec. 4 using cross-validation to determine the optimal hyperparameters. We then compare the results using ROC curves.

6. RESULTS

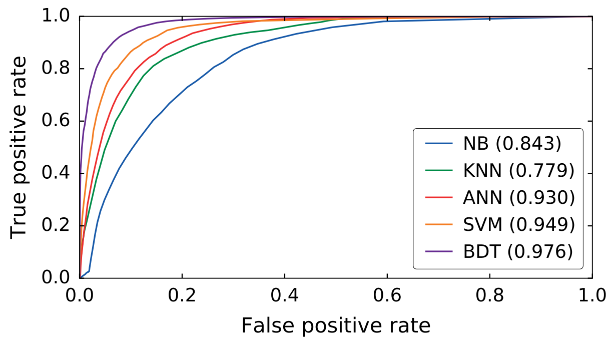

(a) SALT2 model, no redshift

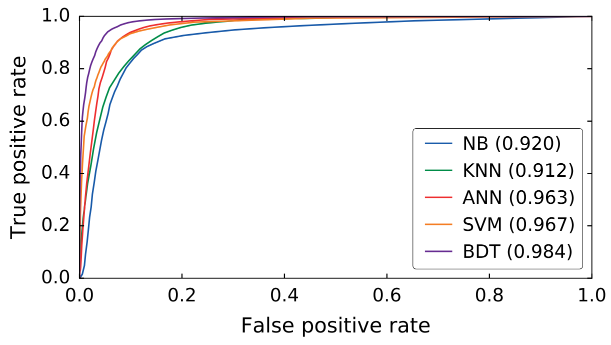

(b) SALT2 model, with redshift

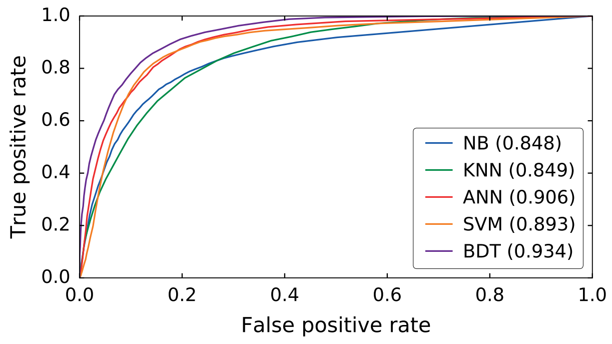

(c) Parametric model 1, no redshift

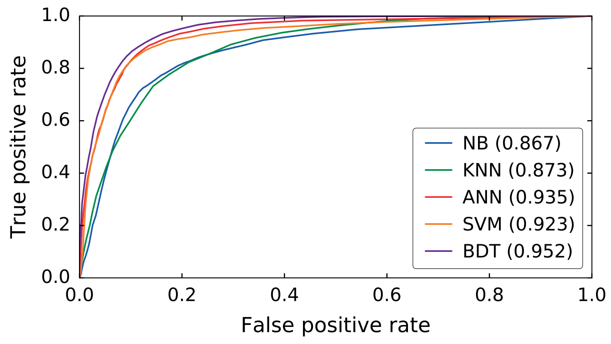

(d) Parametric model 1, with redshift

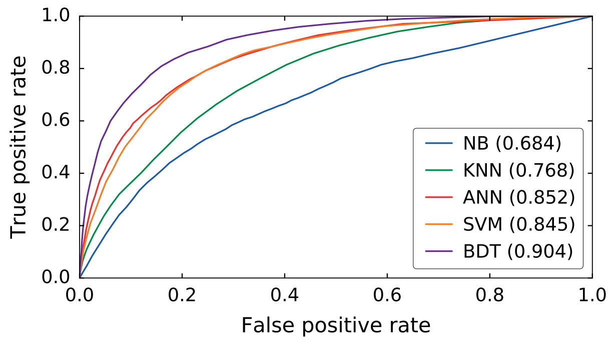

(e) Parametric model 2, no redshift

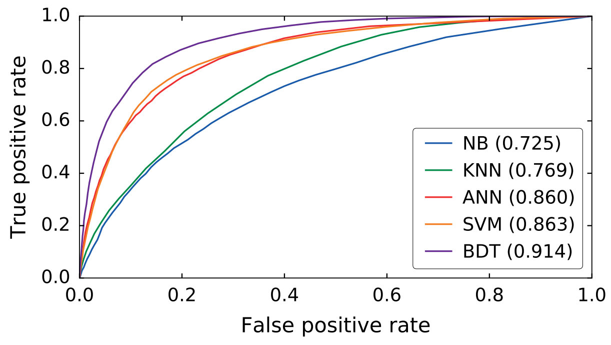

(f) Parametric model 2, with redshift

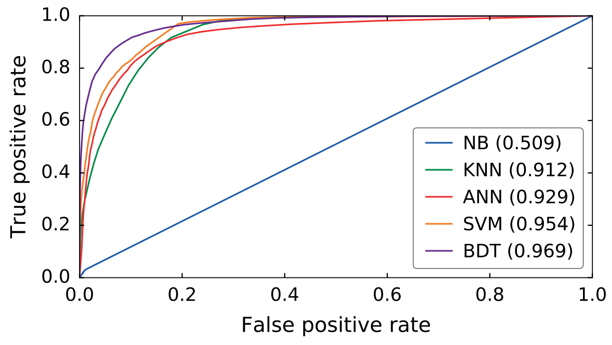

(g) Wavelets, no redshift

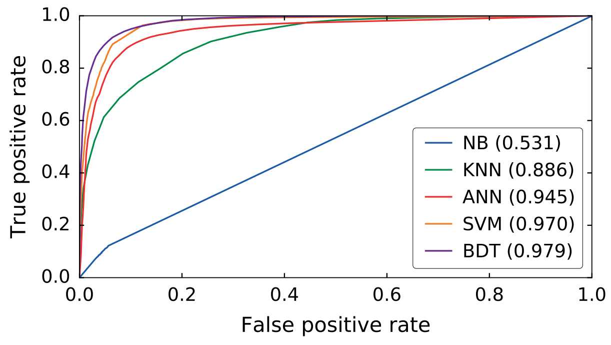

(h) Wavelets, with redshift

Fig. 3.— Receiver operating characteristic (ROC) curves for the various feature extraction methods, using a representative training set without (first column) and with (second column) redshift data included. Each curve represents a different machine learning algorithm (as outlined in Sec. 4) with the area-under-curve (AUC) score in brackets. An AUC of 1 indicates perfect classification and corresponds to a curve close to the top left corner. It is clear that boosted decision trees (BDT), support vector machines (SVM) and artificial neural networks (ANN) are the best-performing algorithms, superior to k-nearest neighbors (KNN) and naive Bayes (NB). The SALT2 and wavelet feature sets provide the best classification.

Figure 3 shows the ROC curves for a representative training set, both without and with redshift information included. From the ROC curves, it is clear that not all machine learning algorithms perform equally and indeed, in every case the boosted decision trees outperform the other algorithms. These ROC curves also illustrate that if the fundamental assumptions of an algorithm are broken, it performs poorly. Naive Bayes performs reasonably well in most cases, but is barely better than random in the case of the wavelets, which are highly non-Gaussian in their distribution. We can also see that the SALT2 features and the wavelet features outperform the parametric models, implying that it is best to use either a highly model-dependent approach, making use of prior knowledge, or with a highly model-independent approach for supernova classification.

Figure 4 shows the Venn diagram for object classification for each of the four feature extraction methods, using boosted decision trees. Objects were classified according to the class with highest probability. From this, one can see that type II supernovae are straightforward to classify, with all feature extraction methods achieving excellent accuracy. Type Ia's are somewhat more difficult, although the SALT2, Model 1 and wavelets methods agree well. There is little agreement between classifiers when it comes to the type Ibc's. This is unsurprising as Ibc light curves are often similar to Ia's and there are relatively few Ibc's in the dataset. The SALT2 method does significantly better than the others at identifying Ibc's.

As stated in Sec. 4.2, the probability threshold at which you select an object's class is arbitrary, meaning that the given class for each supernova will change depending on the threshold used. It is well known that commonly used metrics such as accuracy, purity and completeness are dependent on the threshold used and do not give a complete picture (hence why we advocate the use of the AUC as a comparison metric). However as an example of the values of these metrics for the SPCC dataset, we can vary the threshold probability and insist on a 90% pure type Ia dataset. Then the corresponding completeness is 85%, 41%, 7.8%, 83% for SALT 2, Model 1, Model 2 and wavelets respectively. However, if a more complete dataset is more important, we find that demanding a 90% completeness results in a purity of 87%, 77%, 75%, 87% respectively.

6.1. *The effect of redshift*

The effect of redshift is summarized succinctly in Fig. 5, comparing all feature extraction methods and machine learning algorithms. Figure 5 shows that providing redshift information plays an important role for SALT2 features, mildly improves the results of the parametric features, and is fairly unimportant to the wavelet features. The notable exception to this is when considering the best machine learning algorithm, boosted decision trees. With this algorithm, including redshift information is not essential as the algorithm is capable of differentiating between classes without redshift information.

This raises the interesting point that with an algorithm with poor performance, such as KNN, redshift information is crucial to classify well with the SALT2 model. However, a better machine learning algorithm eliminates the need for redshift information (under the assumption of a representative training set). This is important since obtaining reliable redshifts for every object in future surveys will be challenging. We have shown that it will be possible to obtain a relatively pure subsample of supernovae without redshift information, on which to focus follow-up observations.

It is also interesting to note that the wavelet method, which uses no prior knowledge of supernovae, is able to perform as well as the current state-of-the-art classification technique, based on supernova templates. This is promising since the simulated dataset used here was constructed using largely the same known templates, so it is expected that the SALT2 model should perform well. However, the wavelet approach requires no previous knowledge and so should perform well with new datasets. This also suggests wavelet approaches to classification are likely to be useful for broader transient classification, as also noted in Varughese et al. (2015).

6.2. *The effect of representativeness*

We also investigate the effect of using a representative or non-representative training set. It is well known that most machine learning algorithms underperform when the training set is in any way not representative of the distribution of features. The training set from the SPCC was known to be biased in the way spectroscopic follow-up datasets usually are, in that only the brightest objects tend to be followed up due to telescope time constraints and the difficulty in obtaining good spectra. It is not surprising then that, as shown in Fig. 6, all feature extraction methods and all algorithms perform significantly worse with the non-representative training set. It should be noted that redshift information was not provided here, which only mitigates the effect of non-representativeness in the case of the SALT2 model. This is because the SALT2 model is already based on a large training set of supernovae and thus, if redshift information is given, will produce similar sets of features.

The clear conclusion is that the more representative the training set, the better any classification method will perform. As the training set was only around 5% of the size of the full dataset, we would argue that if spectroscopic follow-up time is limited, it is rather better to obtain fewer, fainter objects of all types, than to get a larger sample of brighter objects.

6.3. *Feature importances*

It is possible to investigate the relative importance of each feature in a feature set using boosted decision trees. This is illustrated for each feature set in Fig. 7, both with and without redshift.

For the SALT2 model, the most important features are the shape and color parameters. Notice that, counterintuitively, the importance of redshift goes *down* when external redshift information is added. By adding redshift information, the Ia's in the dataset are better fit by the SALT2 model as expected, resulting in accurate estimates of the stretch and color parameters. On the other hand, with the redshift fixed the best fits for the non-Ia's result in unphysical stretch and color parameters. Because the distributions of these important features now differ much more between the non-Ia's and Ia's, they increase in importance when classifying. Because all the

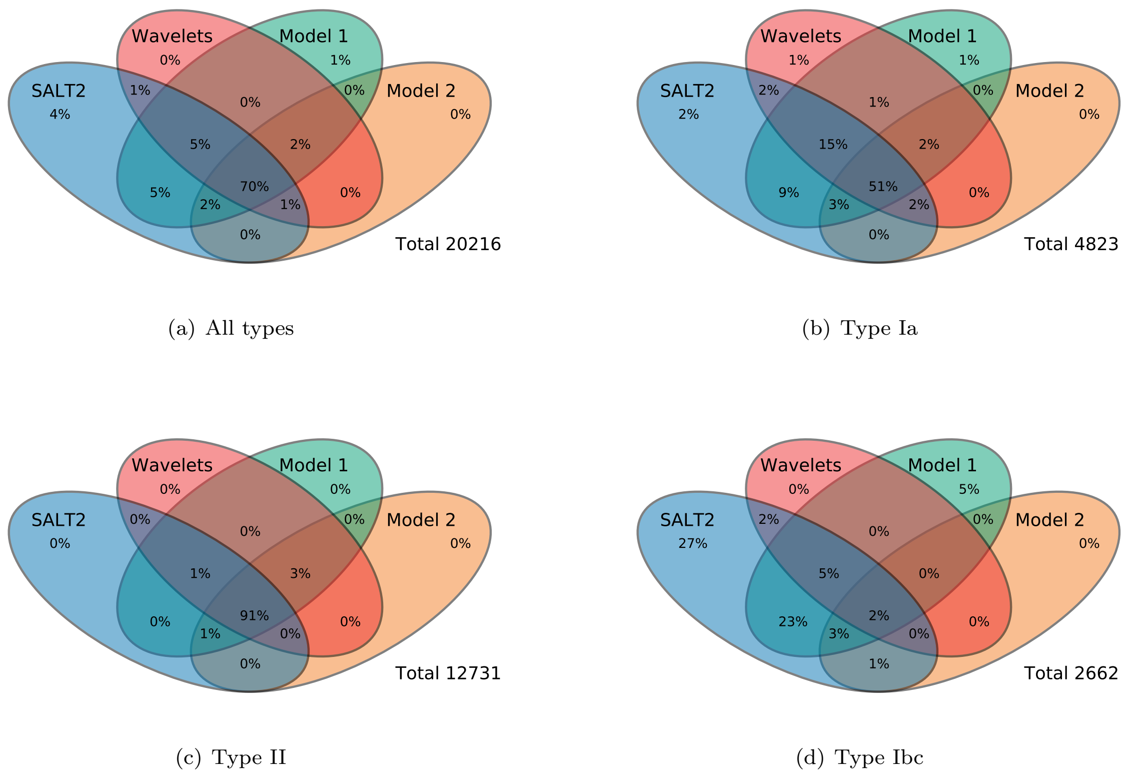

Fig. 4.— Venn diagrams showing the number of correctly classified objects for each feature extraction method using boosted decision trees, with each area indicating the percentage of objects correctly classified. This is repeated for all objects and for each type of supernova individually. It is clear that, for example, type II supernovae are easy to classify, with all feature extraction methods agreeing on the types and achieving excellent accuracy, while type Ibc's are much more difficult to classify.

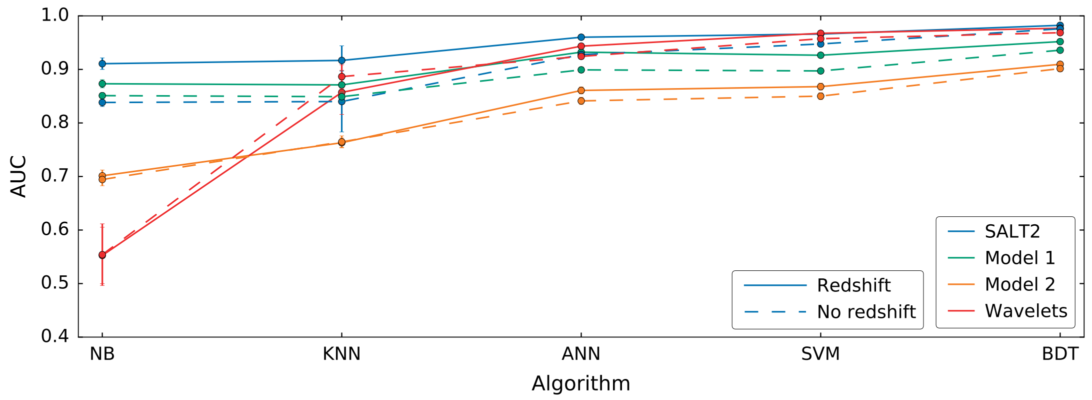

Fig. 5.— Area-under-curve (AUC) as a function of feature set and machine learning algorithm. Higher AUC scores correspond to better classification. Solid lines indicate redshift was included as a feature, while dashed lines represent feature sets without redshift information. The five machine learning algorithms considered are on the x-axis, while each color corresponds to a different feature extraction method. Error bars are from the standard deviation of the AUC from ten runs with randomized training sets. When using BDT, the SALT2 and wavelet features are able to classify equally well with or without redshift. By comparison, the SALT2 features are highly sensitive to redshift when using, for example, the NB or KNN algorithm.

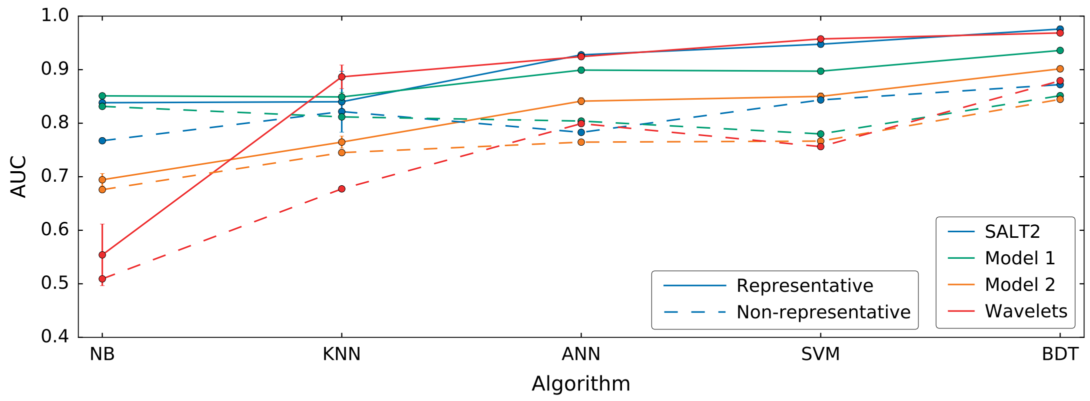

Fig. 6.— Area-under-curve (AUC) as a function of feature set and machine learning algorithm. Higher AUC scores correspond to better classification. Solid lines indicate a representative training set was used, while dashed lines indicate the use of the non-representative training set of Kessler et al. (2010a,b). The five machine learning algorithms considered are on the x-axis, while each color corresponds to a different feature extraction method. Error bars for the representative training set case are the standard deviation from ten runs with randomized training sets. It is clear that any feature extraction method or machine learning algorithm used is highly sensitive to non-representativeness in the training set.

importances must add up to one, this necessarily dictates a decrease in the importance of other features, including the redshift.

There are a few features which are more important for the parametric models, but none notable. Interestingly, it is the third and fourth principal components for the wavelet features which are most important, while all others have fairly equivalent importance.

7. CONCLUSIONS

Classification of photometric supernovae is an important problem in light of current and upcoming surveys. We have compared several different approaches to this problem, some based on current techniques and some new. We have shown that in terms of feature extraction, both SALT2 model fits and wavelet decomposition outperform parametric fits. Out of the five representative machine learning algorithms we used, boosted decision trees performed the best, followed by support vector machines and artificial neural networks. The SALT2 fits and the wavelet approach both achieved an AUC of 0.98, representing excellent classification. The SALT2 and wavelet methods can both produce a dataset that is about 90% pure and 84% complete, although the purity can be increased at the cost of completeness.

Importantly, we found that with a powerful ensemble algorithm like boosted decision trees and a representative training set, redshift information does not improve classification performance, meaning a dataset can be well classified without any redshift information at all. This is extremely useful for current and upcoming surveys where reliable host galaxy photometric redshifts may be difficult to obtain.

Although redshift information is needed for cosmology, this means a well-classified subset of supernovae will be available without any redshift information, with which follow-up studies can be done if necessary. This also implies uncertainties in classification will be completely uncorrelated with uncertainties in redshift estimates. It also means there will be a large sample of robustly classified supernovae available for core collapse research.

On the other hand, with all algorithms and feature extraction methods considered, a representative training set is crucial for good performance. The training set used was very small (around 5% of the dataset) suggesting that a spectroscopic follow-up program should rather focus on observing fainter objects of all types rather than obtaining a larger training set which is not representative.

There are many further improvements one can consider in both the feature extraction methods and the machine learning algorithms. We have provided a framework here for directly and easily comparing these and any future approaches to the photometric supernova classification problem.

In future work we will apply this pipeline to SDSS data and compare against current photometric classifications. Additionally, the pipeline developed here will be crucial in investigating how changes in observing strategy affect classification for LSST.

ACKNOWLEDGMENTS

We thank Michael Betancourt, Rahul Biswas, Saurabh Jha, Bob Nichol, Stephen Smartt and Mark Sullivan for useful discussions. We acknowledge support from STFC for UK participation in LSST through grant ST/N00258X/1 and travel support provided by STFC for UK participation in LSST through grants ST/L00660X/1 and ST/M00015X/1. HVP and ML were supported by the European Research Council under the European Community's Seventh Framework Programme (FP7/2007- 2013) / ERC grant agreement no 306478-CosmicDawn. OL and ML acknowledge a European Research Council Advanced Grant FP7/291329 (TESTDE) and support from STFC.

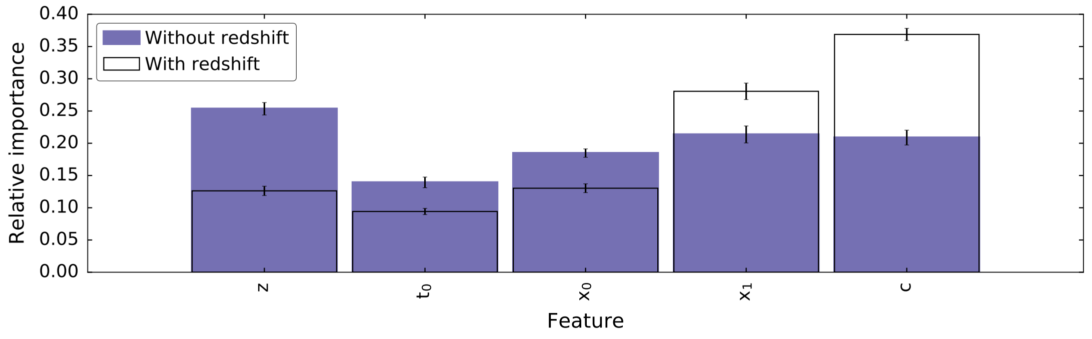

(a) SALT2

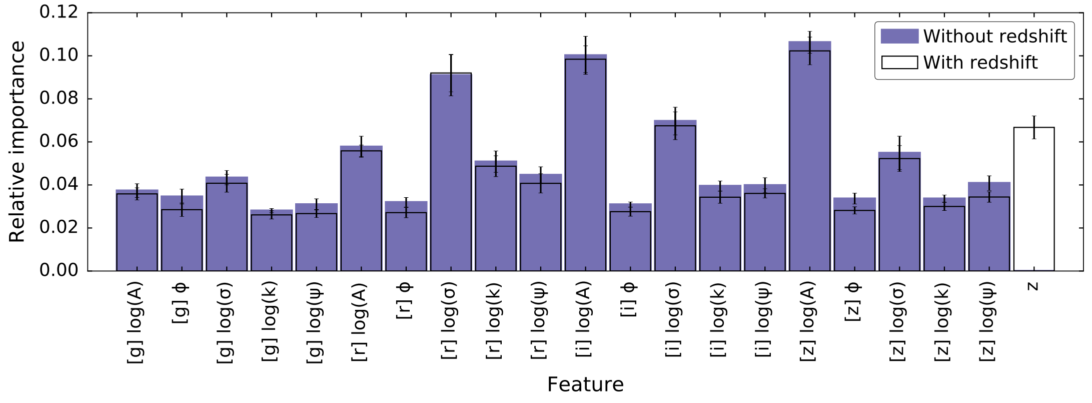

(b) Parametric model 1

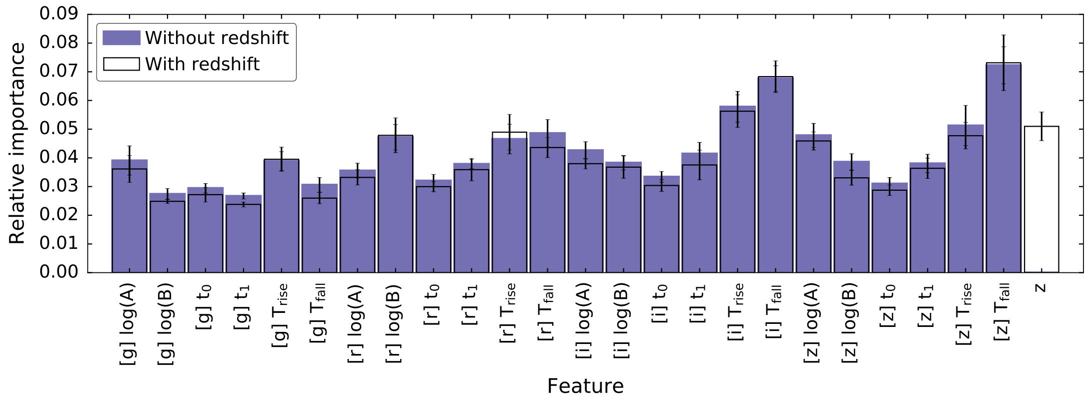

(c) Parametric model 2

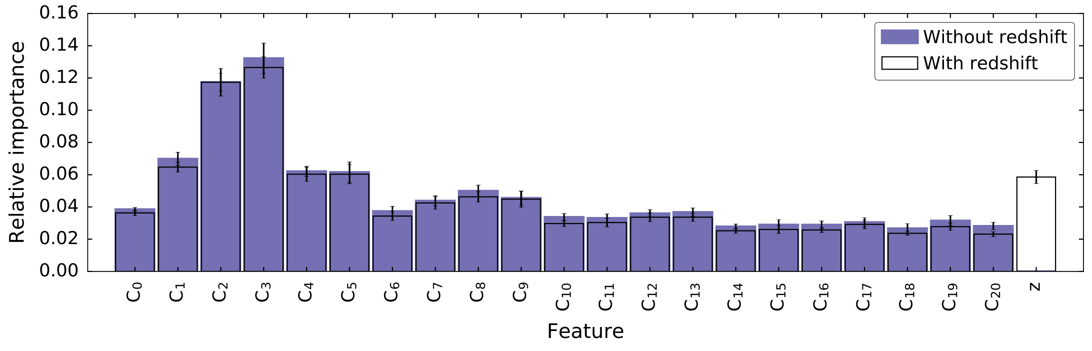

(d) Wavelets

Fig. 7.— Relative importances of individual features with and without redshift information, as obtained from the boosted decision trees algorithm. The SALT2 model is able to estimate the redshift, which is thus still used as a feature even when no redshift information is provided (and a broad, flat prior is used for the fitting). For parametric models 1 and 2, the filter is given in square brackets before the parameter. For the wavelets, the 20 principal components used are labeled C_1 to C_{20}.

REFERENCES

Aızerman, M. 1964, Automation and Remote Control, 25, 821
Altman, N. S. 1992, The American Statistician, 46, 175
Ball, N. M., & Brunner, R. J. 2010, International Journal of Modern Physics D, 19, 1049
Barbary, K. 2014, sncosmo v0.4.2, doi:10.5281/zenodo.11938
Bernstein, J. P., Kessler, R., Kuhlmann, S., et al. 2012, The Astrophysical Journal, 753, 152
Betoule, M., Kessler, R., Guy, J., et al. 2014, Astronomy & Astrophysics, 568, A22
Bloom, J. S., & Richards, J. W. 2012, Data Mining and Machine Learning in Time-Domain Discovery and Classification, 89–112
Breiman, L. 2001, Machine Learning, 45, 5
Breiman, L., Friedman, J., Stone, C. J., & Olshen, R. A. 1984, Classification and regression trees (CRC press)
Buchner, J., Georgakakis, A., Nandra, K., et al. 2014, Astronomy & Astrophysics, 564, A125
Caruana, R., & Niculescu-Mizil, A. 2006, in Proceedings of the 23rd International Conference on Machine Learning, ICML '06 (New York, NY, USA: ACM), 161–168
Cortes, C., & Vapnik, V. 1995, Machine learning, 20, 273
Dark Energy Survey Collaboration. 2005, ArXiv Astrophysics e-prints, astro-ph/0510346
Dark Energy Survey Collaboration, Abbott, T., Abdalla, F. B., et al. 2016, ArXiv e-prints, arXiv:1601.00329
Daubechies, I. 1988, Communications on pure and applied mathematics, 41, 909
Dietterich, T. G. 2000, in Multiple classifier systems (Springer), 1–15
du Buisson, L., Sivanandam, N., Bassett, B. A., & Smith, M. 2015, Monthly Notices of the Royal Astronomical Society, 454, 2026
Fawcett, T. 2004, Machine learning, 31, 1
Feroz, F., & Hobson, M. P. 2008, Monthly Notices of the Royal Astronomical Society, 384, 449
Feroz, F., Hobson, M. P., & Bridges, M. 2009, Monthly Notices of the Royal Astronomical Society, 398, 1601
Feroz, F., Hobson, M. P., Cameron, E., & Pettitt, A. N. 2013, ArXiv e-prints, arXiv:1306.2144
Freund, Y., & Schapire, R. E. 1997, Journal of computer and system sciences, 55, 119
Friedman, J. H. 2002, Computational Statistics & Data Analysis, 38, 367
Frieman et al. 2008, The Astronomical Journal, 135, 338
Green, D., & Swets, J. 1966, Society, 1, 521
Guy, J., Astier, P., Baumont, S., et al. 2007, Astronomy & Astrophysics, 466, 11
Hanley, J. A., & McNeil, B. J. 1982, Radiology, 143, 29
Holschneider, M., Kronland-Martinet, R., Morlet, J., & Tchamitchian, P. 1989, in Wavelets (Springer), 286–297
Hotelling, H. 1933, Journal of educational psychology, 24, 417
J. Newling et al. 2012, Monthly Notices of the Royal Astronomical Society, 421, 913
Jeffrey, W., & Rosner, R. 1986, The Astrophysical Journal, 310, 473
Jha, S., Riess, A. G., & Kirshner, R. P. 2007, The Astrophysical Journal, 659, 122
Karpenka, N. V., Feroz, F., & Hobson, M. P. 2013, Monthly Notices of the Royal Astronomical Society, 429, 1278
Kessler, R., Conley, A., Jha, S., & Kuhlmann, S. 2010a, ArXiv e-prints, arXiv:1001.5210
Kessler, R., Bassett, B., Belov, P., et al. 2010b, Publications of the Astronomical Society of the Pacific, 122, 1415
Kingsbury, N. 2001, Applied and Computational Harmonic Analysis, 10, 234
Knights, M., Bassett, B. A., Varughese, M., et al. 2013, Journal of Cosmology and Astroparticle Physics, 1, 039
Kohavi, R., et al. 1995in , 1137–1145
Li, J., Cheng, K., Wang, S., et al. 2016, ArXiv e-prints, arXiv:1601.07996
Lo, E. H. S., Pickering, M. R., Frater, M. R., & Arnold, J. F. 2009, in Proceedings of the ACM International Conference on Image and Video Retrieval, CIVR '09 (New York, NY, USA: ACM), 5:1–5:8
LSST Science Collaboration. 2009, ArXiv e-prints, arXiv:0912.0201
M. Kunz, B. Bassett and R. Hlozek. 2007, Phys.Rev.D, 75, 103508
MacKay, D. J. 2003, Information theory, inference and learning algorithms (Cambridge university press)
Mallat, S. G. 2009, A wavelet tour of signal processing, 3rd edn. (Burlington: Academic Press)
Morgan, J. N., & Sonquist, J. A. 1963, Journal of the American statistical association, 58, 415
Newling, J., Varughese, M., Bassett, B., et al. 2011, Monthly Notices of the Royal Astronomical Society, 414, 1987
Pearson, K. 1901, The London, Edinburgh, and Dublin Philosophical Magazine and Journal of Science, 2, 559
Pedregosa, F., Varoquaux, G., Gramfort, A., et al. 2011, Journal of Machine Learning Research, 12, 2825
Platt, J., et al. 1999, Advances in large margin classifiers, 10, 61
R. Hlozek et al. 2012, The Astrophysical Journal, 752, 79
Rubin, D., Aldering, G., Barbary, K., et al. 2015, The Astrophysical Journal, 813, 137
Sako, M., Bassett, B., Becker, A., et al. 2008, The Astronomical Journal, 135, 348
Sako, M., Bassett, B., Connolly, B., et al. 2011, The Astrophysical Journal, 738, 162
Sako, M., Bassett, B., Becker, A. C., et al. 2014, ArXiv e-prints, arXiv:1401.3317
Sanders, N. E., Soderberg, A. M., Gezari, S., et al. 2015, The Astrophysical Journal, 799, 208
Seikel, M., Clarkson, C., & Smith, M. 2012, Journal of Cosmology and Astroparticle Physics, 6, 036
Spackman, K. A. 1989, in Proceedings of the sixth international workshop on Machine learning, Morgan Kaufmann Publishers Inc., 160–163
Valens, C. 1999, ed. Clemens Valens
Van der Maaten, L., & Hinton, G. 2008, Journal of Machine Learning Research, 9, 85
Varughese, M. M., von Sachs, R., Stephanou, M., & Bassett, B. A. 2015, Monthly Notices of the Royal Astronomical Society, 453, 2848
Werbos, P. 1974
Wright, D. E., Smartt, S. J., Smith, K. W., et al. 2015, Monthly Notices of the Royal Astronomical Society, 449, 451
Xiong, H., Zhang, T., & Moon, Y. S. 2000, IEEE Transactions on Image Processing, 9, 2100
Zhang, H. 2004, AA, 1, 3

APPENDIX

HYPERPARAMETER SELECTION

Table 5 shows the values of the hyperparameters for each machine learning algorithm for an example case. These hyperparameters are selected using cross-validation (as described in Sec. 4) to maximize the AUC. These values vary slightly depending on training set used.

TABLE 5
Hyperparameters for each machine learning algorithm and each feature set for the case where redshift is included and a representative dataset is used.

	SALT2	Model 1	Model 2	Wavelets
NB	-	-	-	-
KNN	n_neighbors=141	n_neighbors=101	n_neighbors=46	n_neighbors=121
SVM	C=0.56, γ=1.78	C=1780,γ=0.0032	C=31.6,γ=0.0032	C=0.56,γ=1.78
ANN	neurons=110	neurons=110	neurons=115	neurons=80
BDT	n_estimators=40	n_estimators=75	n_estimators=65	n_estimators=70